IMPLEMENTATION OF THE ATLAS-SUSY-2018-06 ANALYSIS IN THE MADANALYSIS 5 FRAMEWORK

J.H. KIM[1], T.G. LEE[2], J.W. KIM[3], H. JANG[4]

[1] *Konkuk University, 120 Neungdong-ro, Gwangjin-gu, Seoul 05029, Korea*
[2] *Department of Physics, Korea University, Seoul 136-713, Korea*
[3] *University of Seoul, 163, Seoulsiripdae-ro, Dongdaemun-gu, Seoul, Republic of Korea*
[4] *Gwangju Institute of Science and Technology, 123, Cheomdangawgi-ro, Buk-gu, Gwangju, Republic of Korea*

We present the MADANALYSIS 5 implementation and validation of the ATLAS-SUSY-2018-06 analysis. This analysis documents a search for electroweakinos with mass splittings larger than the Z boson mass. The targeted decay chain consists of electroweakinos decaying via on-shell W and Z bosons to a three-lepton final state. The results are based on a dataset of 139 fb^{-1} of proton-proton collisions, recorded by the ATLAS experiment with a center-of-mass energy of $\sqrt{s} = 13$ TeV between 2015 and 2018. The validation of our reimplementation relies on a comparison of our results against official cutflows provided by the ATLAS collaboration. The validation material provided by the ATLAS collaboration is based on well-defined benchmarks which feature chargino and neutralino associated production.

1. Introduction

Supersymmetry (SUSY) [1, 2] is an extension of Standard Model (SM) which predicts the existence of spin partners for each SM particle. Some of these partners are the so-called electroweakinos that consist in admixtures of the partners of the neutral and charged gauge and Higgs bosons of the model. In general and as in the analysis considered in this work, the lightest supersymmetric particle (LSP), a candidate of dark matter, is assumed to be the lightest neutralino, $\tilde{\chi}_1^0$.

In this contribution, we present the MADANALYSIS 5 [3–6] implementation of the ATLAS-SUSY-2018-06 [7] search for electroweakinos, together with its validation. The ATLAS analysis is targeting chargino ($\tilde{\chi}_1^\pm$) and neutralino ($\tilde{\chi}_2^0$) production in the case where the spectrum features mass splittings $\Delta m = m(\tilde{\chi}_1^\pm/\tilde{\chi}_2^0) - m(\tilde{\chi}_1^0)$ larger than the Z boson mass, and where the chargino and the second neutralino are mass degenerate. The analysis focuses on a decay chain in which the produced electroweakinos decay into the invisible LSP $\tilde{\chi}_1^0$ and either a W or Z gauge boson. The full decay processes are then $\chi_1^\pm \to \chi_1^0 W^\pm \to \chi_1^0 l^\pm \nu$ and $\chi_2^0 \to \chi_1^0 Z \to \chi_1^0 l^+ l^-$. Finally, both the W and Z bosons decay leptonically, which leads to a final-state signature comprised of three leptons and the missing transverse momentum originating from two LSPs and a neutrino. This process is illustrated in Figure 1.

The conventional method which uses laboratory-frame when reconstructing the

2   *J.H Kim, T.G Lee, J.W Kim, H. Jang*

SUSY particles has some ambiguities. If the LSP is produced at colliders, it will leave the detectors without interacting. Thus, its presence can only be inferred from the missing momentum vector. However, this is problematic in that, not only the information of the properties of the final state is lost, but also the information of the intermediate particles is lost. For the SUSY particles with multiple decays, it can be difficult to match the decay products, which are indistinguishable, and reconstruct the originally produced particles without this information. This results in ambiguities when reconstructing the potentially produced electroweakinos $\tilde{\chi}_1^{\pm}$, $\tilde{\chi}_2^0$.

The recursive jigsaw reconstruction (RJR) technique [8,9] has been proposed to resolve these ambiguities by analyzing each event starting from the laboratory-frame particles and boosting back to the rest frames of the pair-produced parent sparticles (PP frame). Using this technique, the ATLAS collaboration found excesses of three lepton events in two regions in 36.1 fb^{-1} of data collected between 2015 and 2016 [10]. In this last analysis, one region, named SR-LOW, has led to a local significance of 2.1σ and targeted low-mass ($\tilde{\chi}_1^{\pm}$ $\tilde{\chi}_2^0$) production. Another region, named SR-ISR (initial state radiation), yielded a local significance of 3.0σ and targeted $\tilde{\chi}_1^{\pm}$ $\tilde{\chi}_2^0$ production associated with an initial-state radiation (ISR). Thus, further analysis was made in ATLAS-SUSY-2018-06 with higher luminosity of 139 fb^{-1}.

In the ATLAS-SUSY-2018-06 analysis, a new approach was made to find the intersection between the conventional and the RJR approach. This new technique emulates the variables used in the RJR approach with laboratory frame variables and using minimal assumptions about the mass of the invisible system. This technique provides a simple set of variables that are easily reproducible. When defining the object and region, the emulated recursive jigsaw reconstruction (eRJR) variables are kept as close as possible with [10]. The eRJR technique was validated by reproducing the excesses of three-lepton events using the same 36.1 fb^{-1} of pp collision data. In the ATLAS-SUSY-2018-06 analysis, this technique is applied to an integrated luminosity of 139 fb^{-1} of pp collision data collected between 2015 and 2018. In this higher luminosity upgrade of the work of [10], the number of events and the number of expected background events in the SR-LOW region are 51 and 46 ± 5, whereas in the SR-ISR region, the number of events and the number of expected background events are 30 and 23.4 ± 2.1.

2. Description of the analysis

The analysis is targeting chargino ($\tilde{\chi}_1^{\pm}$) and neutralino ($\tilde{\chi}_2^0$) production, where they are assumed to respectively decay with a 100% branching ratio into W and Z bosons. Thus, the analysis requires three leptons in the final state. After defining the signal objects, eRJR variables are computed for each event passing some preselection. Those different eRJR variables are then used to define two different classes of signal regions, SR-LOW and SR-ISR, as further detailed in section 2.2.
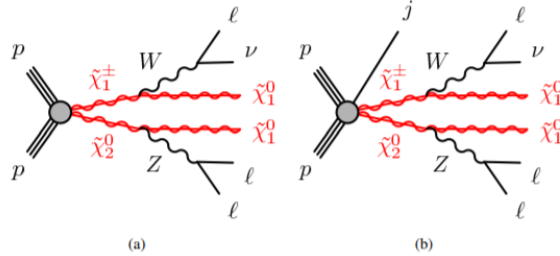
Fig. 1. Representative Feynman diagram corresponding to $\tilde{\chi}_1^{\pm}$ $\tilde{\chi}_2^0$ production with subsequent decays into two $\tilde{\chi}_1^0$ via leptonically decaying W and Z bosons. The final-state signature is thus comprised of three leptons and a neutrino. Diagrams are shown both (a) without a jet and (b) with a jet originating from initial-state QCD radiation.

2.1. *Object definitions*

Electron candidates are required to have a transverse momentum p_T and pseudo-rapidity η satisfying

$$p_\mathrm{T} > 10\,\mathrm{GeV} \qquad \text{and} \qquad |\eta| < 2.47. \qquad (1)$$

To isolate electrons from any additional activity, requirements are imposed using energy clusters in the electromagnetic calorimeter and restrict the activity in a cone of radius $\Delta R = 0.2$ around the electron. Moreover, the sum of transverse energy of the calorimeter energy clusters and the sum of the p_T of all tracks within the cone is constrained to be below 6% of the electron p_T.

Muon candidates are reconstructed with the following requirement,

$$p_\mathrm{T} > 10\,\mathrm{GeV} \qquad \text{and} \qquad |\eta| < 2.4. \qquad (2)$$

Muons must also be isolated from any additional activity and their isolation is defined similarly as for the electrons. For muons with $p_\mathrm{T} < 33$ GeV, the isolation cone radius is $\Delta R = 0.3$. In the case of muons with p_T larger than 33 GeV, ΔR decreases linearly as a function of p_T, and terminates to $\Delta R = 0.2$ at $p_\mathrm{T} = 50$ GeV. For muons with p_T larger than 50 GeV, the isolation cone is maintained as $\Delta R = 0.2$. The sum of transverse energy of the calorimeter energy clusters within the cone should be below 15% of the muon p_T. Furthermore, the sum of the p_T of all tracks within the cone is constrained to be below 4% of the muon p_T.

Jets are reconstructed using the anti-k_t algorithm [11] with reconstruction radius of $R = 0.4$. Jets whose p_T is larger than 20 GeV and $|\eta| < 2.4$ are considered as signal jets.

For the unique identification of leptons and jets, an overlap removal procedure is implemented. Electrons are removed if they are within $\Delta R = 0.2$ of a muon. Jets are discarded if they are within $\Delta R = 0.2$ of a lepton. Finally, leptons with $p_\mathrm{T} \leq 25$ GeV are removed if their angular distance from jet is $\Delta R < 0.4$. For leptons with $p_\mathrm{T} \geq 25$ GeV, this angular distance (ΔR) decreases as a linear function of p_T to $\Delta R < 0.2$ as p_T increases from $p_\mathrm{T} = 25$ GeV to $p_\mathrm{T} = 50$ GeV.

4 *J.H Kim, T.G Lee, J.W Kim, H. Jang*

2.2. *Event selection*

Event selection is performed using different eRJR variables. Five different eRJR variables are used to define the SR-ISR region. The first of them consists in the missing transverse energy $E_{\mathrm{T}}^{\mathrm{miss}}$ that is defined as the magnitude of the missing transverse momentum. The second variable is the magnitude of the transverse momentum of jets $p_{\mathrm{T}}^{\mathrm{jets}}$ that is defined as the magnitude of the vector sum of the signal jets' transverse momenta. This variable is calculated as

$$p_{\mathrm{T}}^{\mathrm{jets}} = p \left(\sum_{i=1}^{N} \mathbf{p}_i^{\mathrm{jets}} \right)_{\mathrm{T}}, \tag{3}$$

where N is the number of reconstructed signal jets. We defined $p(\mathbf{X})_{\mathrm{T}}$ as the magnitude of the transverse momentum of the vector $\mathbf{X}$ in the parentheses. The third variable $\Delta\phi(E_{\mathrm{T}}^{\mathrm{miss}}, \mathrm{jets})$ is the azimuthal angle between the missing transverse momentum vector and the vector sum of the signal jets' momenta. The fourth variable is $R(E_{\mathrm{T}}^{\mathrm{miss}}, \mathrm{jets})$, the ratio of the missing transverse momentum to the total transverse momenta of jets, is calculated as

$$R(E_{\mathrm{T}}^{\mathrm{miss}}, \mathrm{jets}) \ = \ |\mathbf{p}_{\mathrm{T}}^{\mathrm{miss}} \cdot \mathbf{p}_{\mathrm{T}}^{\mathrm{jets}}| / (\mathbf{p}_{\mathrm{T}}^{\mathrm{jets}} \cdot \mathbf{p}_{\mathrm{T}}^{\mathrm{jets}}), \tag{4}$$

where $\mathbf{p}_{\mathrm{T}}^{\mathrm{miss}}$ is the missing transverse momentum and $\mathbf{p}_{\mathrm{T}}^{\mathrm{jets}}$ is the vector sum of transverse momenta of jets. The last variable that is used to define the SR-ISR is $p_{\mathrm{T}}^{\mathrm{soft}}$ which is defined as the p_T in the vector sum of the four-momenta of the signal jets, leptons and the missing transverse momentum,

$$p_T^{\mathrm{soft}} = p(\mathbf{p}^{\mathrm{leptons}} + \mathbf{p}^{\mathrm{jets}} + \mathbf{p}_{\mathrm{T}}^{\mathrm{miss}})_{\mathrm{T}}, \tag{5}$$

where $\mathbf{p}^{\mathrm{leptons}}$ is the vector sum of the four-momenta of the leptons.

There are also three different eRJR variables that are used to define the SR-LOW region. The first variable is $p_{\mathrm{T}}^{\mathrm{soft}}$ which has the same name as the one introduced in the SR-ISR region. However, it is defined differently in the SR-LOW region due to a jet veto. $p_{\mathrm{T}}^{\mathrm{soft}}$ is defined as the p_{T} of the vector sum of the four-momenta of the signal leptons and the missing transverse momentum,

$$p_T^{\mathrm{soft}} = p(\mathbf{p}^{\mathrm{leptons}} + \mathbf{p}_{\mathrm{T}}^{\mathrm{miss}})_{\mathrm{T}}. \tag{6}$$

The second variable is m_{eff}^{3l} and it is defined as the scalar sum of the p_{T} of the signal leptons and the missing transverse energy,

$$m_{\mathrm{eff}}^{3l} = \left(\sum_{i}^{3} p_{i,\mathrm{T}}^{\mathrm{lepton}} \right) + E_{\mathrm{T}}^{\mathrm{miss}}, \tag{7}$$

where $p_{i,\mathrm{T}}^{\mathrm{lepton}}$ is the transverse momentum of each lepton The last variable that is used in the SR-LOW region is H^{boost} that is defined as the scalar sum of the momentum of the signal leptons and the missing-momentum vector after applying a boost to the rest frame of the pair-produced parent sparticles (PP frame),

$$H^{\mathrm{boost}} = \left(\sum p_{i,\mathrm{T}}^{\mathrm{PP,lepton}} \right) + E_{\mathrm{T}}^{\mathrm{PP,miss}}, \tag{8}$$

where $p_{i,\mathrm{T}}^{\mathrm{PP,lepton}}$ and $E_{\mathrm{T}}^{\mathrm{PP,miss}}$ is the transverse momentum of each lepton and the missing transverse momentum in the PP frame. In order to calculate H^{boost}, two more variables should be determined. Firstly, the longitudinal component of the missing-momentum vector, $p_{||}^{\mathrm{miss}}$, is calculated as

$$p_{||}^{\mathrm{miss}} = p_{\mathrm{V},||} \frac{|\mathbf{p}_{\mathrm{T}}^{\mathrm{miss}}|}{\sqrt{(p_{\mathrm{V,T}})^2 + (m_{\mathrm{V}})^2}}, \tag{9}$$

where $p_{\mathrm{V},||}$ is the z-component of the vector sum of the four-momenta of the three signal leptons, $p_{\mathrm{V,T}}$ is the p_{T} of the vector sum of the four-momenta of three leptons, and m_{V} is the mass of the three-lepton system. Secondly, the boost of the system is calculated as

$$\beta = \frac{\mathbf{p}}{\mathrm{E}} = \frac{\mathbf{p}^{\mathrm{V}} + \mathbf{p}^{\mathrm{miss}}}{\mathrm{E}^{\mathrm{V}} + |\mathbf{p}^{\mathrm{miss}}|}, \tag{10}$$

where $\mathbf{p}^{\mathrm{V}}$ is the vector sum of the three-momenta of three leptons, which is calculated in the laboratory frame.

2.2.1. *Preselection*

Two different signal regions are defined with different constraints. However, there are some common constraints for both regions. Events are required to feature three signal leptons with at least one pair of leptons with the same-flavor and a different electric charge (SFOS). In addition, the invariant mass m_{ll} of this lepton pair is required to be within $[75, 105]$ GeV. If there exists more than one SFOS pair, the pair is chosen so that its invariant mass is the closest to the Z boson mass. Moreover, the invariant mass of the three-lepton system should be larger than 105 GeV. In order to reduce the contribution from the top backgrounds, a b-jet veto is applied. Finally, to reduce the contribution from the W and Z boson backgrounds, m_{T} should be larger than 100 GeV, where m_{T} is the transverse momentum of the system that is made of the unpaired third lepton and $E_{\mathrm{T}}^{\mathrm{miss}}$. It is calculated as

$$m_{\mathrm{T}} = \sqrt{2 p_{\mathrm{T}} E_{\mathrm{T}}^{\mathrm{miss}} (1 - \cos{(\Delta\phi)})}, \tag{11}$$

where $\Delta\phi$ is the azimuthal separation between the unpaired third lepton and the missing transverse momentum.

2.2.2. *The SR-LOW low-mass region*

In the low-mass region, SR-LOW, there should be no signal jet. To reduce the background from fake or non-prompt leptons, the transverse momenta of three leptons should satisfy

$$p_{\mathrm{T}}^{\mathrm{l_1}} > 60\,\mathrm{GeV} \quad , \quad p_{\mathrm{T}}^{\mathrm{l_2}} > 40\,\mathrm{GeV} \quad \text{and} \quad p_{\mathrm{T}}^{\mathrm{l_3}} > 30\,\mathrm{GeV}. \tag{12}$$

6 *J.H Kim, T.G Lee, J.W Kim, H. Jang*

Moreover, to reduce the contribution from the W and Z boson backgrounds, H^{boost} should be larger than 250 GeV. To further reduce the WZ contribution, p_T^{soft} and m_{eff}^{3l} should satisfy

$$\frac{p_T^{\text{soft}}}{p_T^{\text{soft}} + m_{\text{eff}}^{3l}} < 0.05 \quad \text{and} \quad \frac{m_{\text{eff}}^{3l}}{H^{\text{boost}}} > 0.9. \tag{13}$$

2.2.3. *The SR-ISR initial-state radiation region*

In the SR-ISR region, there should be at least one signal jet as this region has been designed to target the production of an electroweakino pair in association with a hard initial-state radiation jet. $p_T^{\text{soft}} < 25$ GeV together with jet multiplicity smaller than four ($N_{\text{jets}} < 4$) is imposed to reduce the contribution from the WZ backgrounds. The transverse momenta of three leptons should satisfy

$$p_T^{l_1} > 25 \text{ GeV} \quad , \quad p_T^{l_2} > 25 \text{ GeV} \quad \text{and} \quad p_T^{l_3} > 20 \text{ GeV}. \tag{14}$$

In addition, $E_T^{\text{miss}} \geq 80$ GeV reduces the contamination from the Z+jets events. Moreover, the azimuthal separation between the missing transverse momentum and the vector sum of the momenta of the signal jets, $\Delta\phi(E_T^{\text{miss}}, \text{jets})$, should be larger than 2. To reduce the contribution from the WZ backgrounds, the ratio of the transverse momentum to the total transverse momenta of jets, $R(E_T^{\text{miss}}, \text{jets})$, should be within (0.55 , 1.0). Background contamination is further reduced by the requirement of $p_T^{\text{jets}} > 100$ GeV.

3. Validation

3.1. *Event generation*

Our benchmark points are defined by a spectrum featuring $M(\tilde{\chi}_1^\pm/\tilde{\chi}_2^0) = 200$ GeV, $M(\tilde{\chi}_1^0) = 100$ GeV and the masses of the other SUSY particles in the model are set to 5 TeV. In order to validate our analysis, we generated signal samples relevant for a few benchmark scenarios and compared the predictions with the cutflows included in the original paper. Signal samples were generated via MG5_aMC v2.6.7 [12] at leading order(LO) with the LO sets of NNPDF2.3 parton densities [13]. We used the MSSM-SLHA2 [14] model file shipped with MG5_aMC. We generated events by combining samples associated with the $p\,p \rightarrow \chi_1^\pm \chi_2^0$, $\chi_1^\pm \chi_2^0 + j$ and $\chi_1^\pm \chi_2^0 + 2j$ processes, the $\chi_1^\pm \chi_2^0$ decay to $\chi_1^0 W^\pm \chi_1^0 Z$ being enforced to occur with a branching ratio of 1. The decay process were done when simulating parton showering. Parton showering was simulated by PYTHIA 8.244 [15]. For the merging of the multi-partonic matrix elements, we used the MLM technique with the parameters `Xqcut` = 50 GeV in MG5_aMC and `qCut` = 75 GeV in PYTHIA 8. DELPHES 3.4.2 [16] was used to emulate the ATLAS detector. The isolation and unique identification modules in DELPHES 3 were not used and those were done at the analysis level. For jet clustering, we used FASTJET [17] and its implementation of the anti-k_t algorithm with a

radius parameter R = 0.4. The b-tagging efficiency input in DELPHES was provided as a function of p_T extracted from the data collected from 2015 to 2017 [18].

3.2. *Comparison with the official results*

Table 1 and Table 2 compares MADANALYSIS 5 (MA5) cutflow predictions with the ATLAS official results for two signal regions. The relative difference (Δ) between the results from MA5 and the ATLAS ones is computed as,

$$|\Delta| = \left| 1 - \frac{\epsilon_i^{\mathrm{MA5}}}{\epsilon_i^{\mathrm{ATLAS}}} \right| \times 100. \tag{15}$$

The index i corresponds to the cut number, and $\epsilon_i^{\mathrm{MA5}}$ and $\epsilon_i^{\mathrm{ATLAS}}$ refers to the corresponding efficiencies,

$$\epsilon_i = \frac{(\mathrm{Cut})_i}{(\mathrm{Cut})_{i-1}}, \tag{16}$$

where $(\mathrm{Cut})_i$ is the number of events remaining after applying the ith cut. For both signal regions, we observed an agreement of order of up to 10% at every step of each cutflow. In the case of the SR-LOW region, the largest observed discrepancy is related to p_T^{soft}, which was 17.1%. For the case of the SR-ISR region, the largest discrepancy is related to m_T, which was 18.8%. For both regions, large discrepancies are likely to start from the cutflow that strongly rely on jets. That is, the large discrepancies tend to start, in the case of the SR-LOW region, at the jet veto level and in the case of the SR-ISR region, at the cut on N_{jets}. Those discrepancies are thought to be related to the lack of exact information about jet energy scale and jet efficiency that is needed when reconstructing jets in the DELPHES 3 level. We could therefore not further investigate the reasons for the differences.

Figure 2 and Figure 3 compare the distribution of variables that is predicted by MADANALYSIS 5 with official data [19] that is provided by the ATLAS collaboration for the two regions (SR-LOW and SR-ISR). The dotted lines represents the ATLAS official results and the solid lines are the MADANALYSIS 5 predictions. To be specific, Figure 2 compares the distribution of variables in the SR-LOW region: m_T, H^{boost}, $m_{\mathrm{eff}}^{3l}/H^{\mathrm{boost}}$ and $p_T^{\mathrm{soft}}/(p_T^{\mathrm{soft}} + m_{\mathrm{eff}}^{3l})$. The entire SR-LOW event selection is applied for each distribution with the exception of the variable shown. Similarly, Figure 3 compares distributions in the SR-ISR region: m_T, $R(E_T^{\mathrm{miss}}, \mathrm{jets})$, p_T^{soft} and p_T^{jets}. The entire SR-ISR event selection is applied for each distribution of variables with the exception of the shown variable. The remaining events after applying the event selections were quite small, which caused large differences at some point. However, the shape of the histograms matched fairly well with the data provided by the ATLAS collaboration, especially for the SR-LOW region. In the case of the SR-ISR region, large discrepancies were again observed for the variables that strongly rely on jets. The limitation of information about jet reconstruction is thought to be an issue, which is consistent with the results of the cutflow. However, considering the large uncertainties of the data that is provided by the ATLAS collaboration and the

8   *J.H Kim, T.G Lee, J.W Kim, H. Jang*

Table 1.   Comparison of the cutflow predicted by MA5 with the results provided by the ATLAS collaboration for the SR-LOW region.

Cuts	ATLAS(Official)	MA5	difference (Δ)
3 leptons & SFOS	-	-	-
b-jet veto	0.963	0.992	3.0%
$m_{3l} > 105$ GeV	0.970	0.959	1.1%
lepton $p_{\rm T} > 60, 40, 30$ GeV	0.352	0.301	14.5%
$m_{ll} \in [75, 105]$ GeV	0.982	0.985	0.3%
jet veto	0.485	0.564	16.3%
$H^{\rm boost} > 250$ GeV	0.712	0.724	1.7%
$p_{\rm T}^{\rm soft}/(p_{\rm T}^{\rm soft} + m_{\rm eff}^{3l}) < 0.05$	0.712	0.590	17.1%
$m_{\rm eff}^{3l}/H^{\rm boost} > 0.9$	0.651	0.595	8.6%
$m_{\rm T} > 100$	0.392	0.356	9.2%

Table 2.   Comparison of the cutflow predicted by MA5 with the results provided by the ATLAS collaboration for the SR-ISR region.

Cuts	ATLAS(Official)	MA5	difference (Δ)
3 leptons & SFOS	-	-	-
b-jet veto	0.963	0.992	3.0%
$m_{3l} > 105$ GeV	0.970	0.959	1.1%
lepton$p_{\rm T} > 25, 25, 20$ GeV	0.800	0.749	6.4%
$m_{ll} \in [75, 105]$ GeV	0.977	0.976	0.1%
$N_{\rm jets} \in [1, 3]$	0.467	0.408	12.6%
$|\Delta\phi(E_{\rm T}^{\rm miss}, {\rm jets})| > 2.0$	0.672	0.671	0.1%
$R(E_{\rm T}^{\rm miss}, {\rm jets}) \in [0.55, 1.0]$	0.331	0.355	7.3%
$p_{\rm T}^{\rm jets} > 100$ GeV	0.551	0.509	7.6%
$E_{\rm T}^{\rm miss} > 80$ GeV	0.956	0.965	0.9%
$m_{\rm T} > 100$ GeV	0.425	0.505	18.8%
$p_{\rm T}^{\rm soft} < 25$ GeV	0.764	0.696	8.9%

small number of events remaining after the cutflow, our MA5 data could be said to fit with the data provided by the ATLAS collaboration fairly well.

The figures also include the relative difference ($\delta_{\rm rel}$) between the MA5 and the ATLAS predictions, that is calculated by using

$$\delta_{\rm rel} = \left| \frac{N^{\rm ATLAS} - N^{\rm MA5}}{N^{\rm ATLAS}} \right|. \tag{17}$$

For the points where $N^{\rm ATLAS} = 0$, we let $\delta_{\rm rel} = 0$ for convenience. $N^{\rm ATLAS}$ and $N^{\rm MA5}$ refers to the number of events in the ATLAS and the MA5 sequentially.
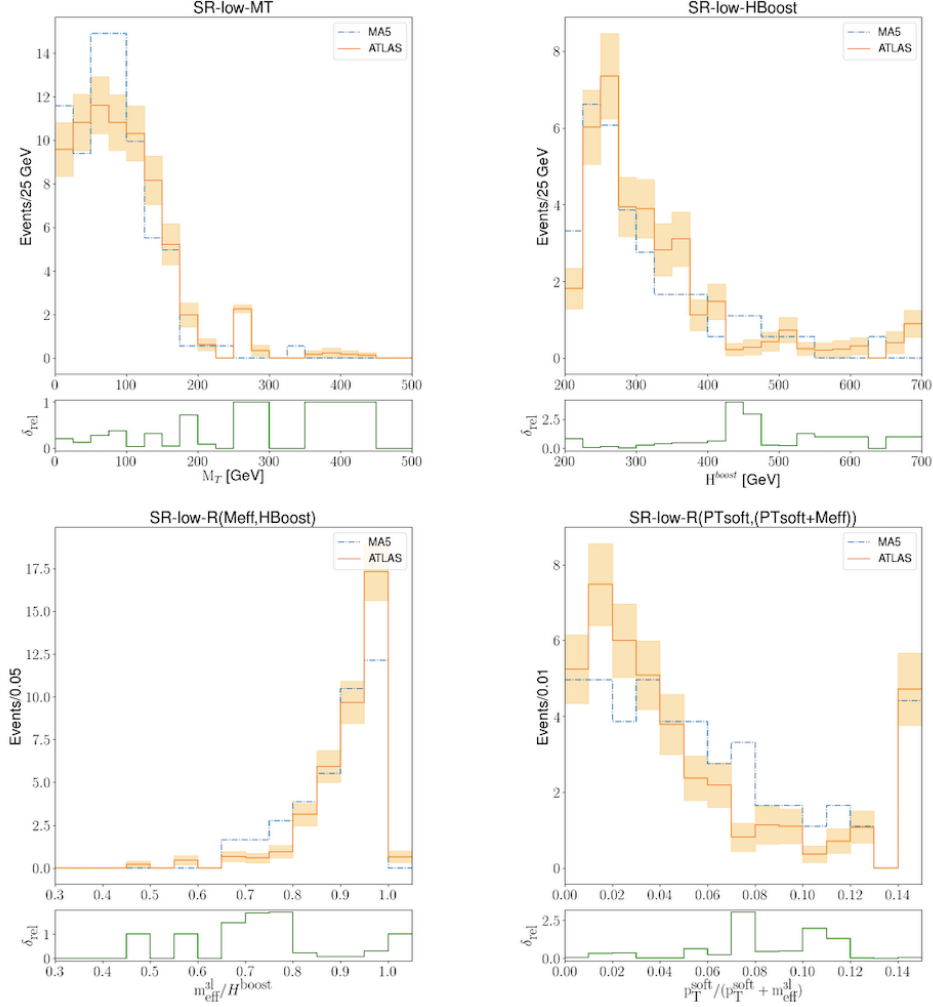
Fig. 2.   Comparison of several differential distributions as predicted by MadAnalysis 5 with the official results provided by the ATLAS collaboration, for the SR-LOW region. The official results provided by the ATLAS collaboration are shown with their uncertainties. The SR-LOW event selections are applied for each distribution except for the variable shown.

4. Conclusions

The MadAnalysis 5 implementation of the ATLAS-SUSY-2018-06 analysis, a search for the production of electroweakinos with the three-lepton final state has been presented. The ATLAS collaboration found excesses of three-lepton events in two signal regions, the low-mass region SR-LOW, and the initial-state radiation region SR-ISR. Validation was done by comparing the efficiency of various selection cuts that has been provided by the ATLAS collaboration with the result predicted by the MA5 framework. We found that the difference between the two was quite
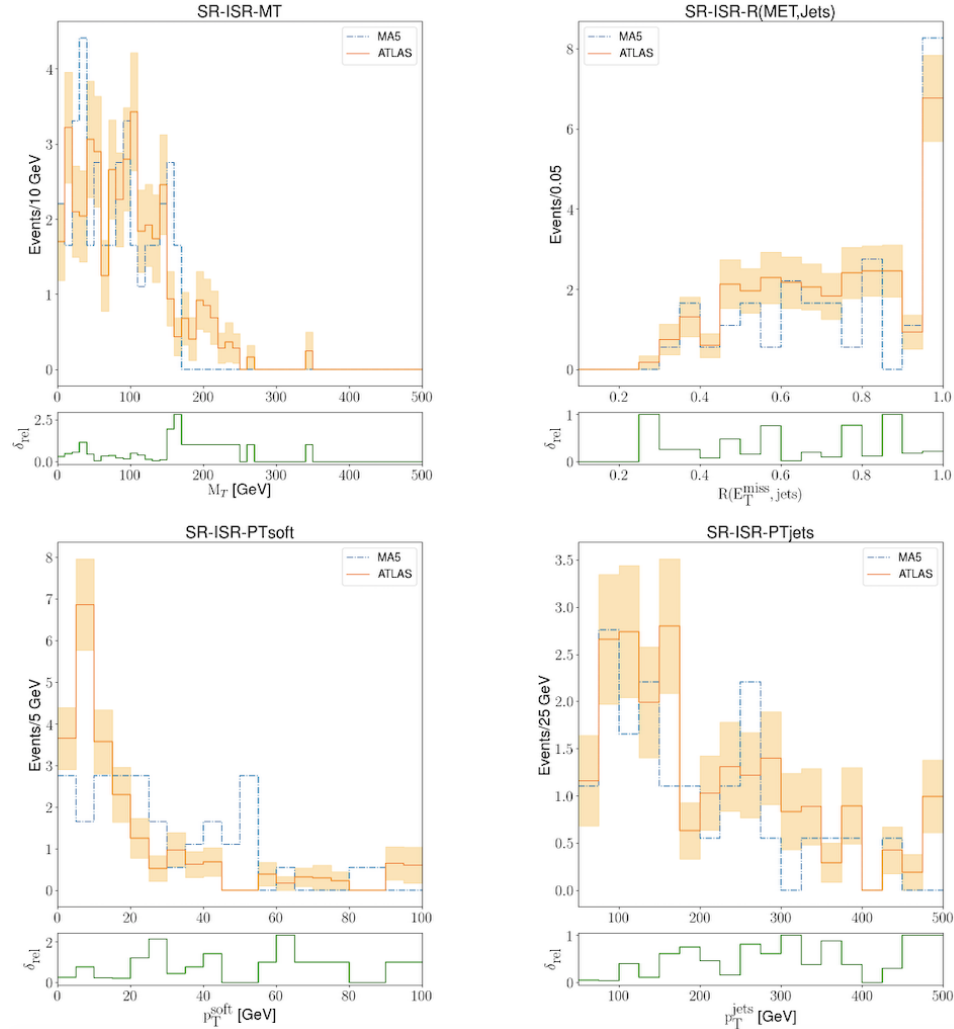
Fig. 3. Comparison of several differential distributions as predicted by MADANALYSIS 5 with the official results provided by the ATLAS collaboration, for the SR-ISR region. The official results provided by the ATLAS collaboration are shown with their uncertainties. The SR-ISR event selections are applied for each distribution except for the variable shown.

acceptable with differences at the level of at most 20%. Thus, we concluded that the analysis reimplementation is validated. The material that has been used for the validation of this implementation is available, together with the MADANALYSIS 5 C++ code, at the MA5 dataverse (https://doi.org/10.14428/DVN/LYQMUJ) [20].

Acknowledgments

References

1. H. P. Nilles, *Phys. Rept.* **110**, 1 (1984).
2. H. E. Haber and G. L. Kane, *Phys. Rept.* **117**, 75 (1985).
3. E. Conte and B. Fuks, *Int. J. Mod. Phys. A* **33**, 1830027 (2018), `arXiv:1808.00480 [hep-ph]`.
4. B. Dumont, B. Fuks, S. Kraml, S. Bein, G. Chalons, E. Conte, S. Kulkarni, D. Sengupta and C. Wymant, *Eur. Phys. J. C* **75**, 56 (2015), `arXiv:1407.3278 [hep-ph]`.
5. E. Conte, B. Dumont, B. Fuks and C. Wymant, *Eur. Phys. J. C* **74**, 3103 (2014), `arXiv:1405.3982 [hep-ph]`.
6. E. Conte, B. Fuks and G. Serret, *Comput. Phys. Commun.* **184**, 222 (2013), `arXiv:1206.1599 [hep-ph]`.
7. ATLAS Collaboration, G. Aad *et al.*, *Phys. Rev. D* **101**, 072001 (2020), `arXiv:1912.08479 [hep-ex]`.
8. P. Jackson, C. Rogan and M. Santoni, *Phys. Rev. D* **95**, 035031 (2017), `arXiv:1607.08307 [hep-ph]`.
9. P. Jackson and C. Rogan, *Phys. Rev. D* **96**, 112007 (2017), `arXiv:1705.10733 [hep-ph]`.
10. ATLAS Collaboration, M. Aaboud *et al.*, *Phys. Rev. D* **98**, 092012 (2018), `arXiv:1806.02293 [hep-ex]`.
11. M. Cacciari, G. P. Salam and G. Soyez, *JHEP* **04**, 063 (2008), `arXiv:0802.1189 [hep-ph]`.
12. J. Alwall, R. Frederix, S. Frixione, V. Hirschi, F. Maltoni, O. Mattelaer, H. S. Shao, T. Stelzer, P. Torrielli and M. Zaro, *JHEP* **07**, 079 (2014), `arXiv:1405.0301 [hep-ph]`.
13. NNPDF Collaboration, R. D. Ball *et al.*, *JHEP* **04**, 040 (2015), `arXiv:1410.8849 [hep-ph]`.
14. C. Duhr and B. Fuks, *Comput. Phys. Commun.* **182**, 2404 (2011), `arXiv:1102.4191 [hep-ph]`.
15. T. Sjöstrand, S. Ask, J. R. Christiansen, R. Corke, N. Desai, P. Ilten, S. Mrenna, S. Prestel, C. O. Rasmussen and P. Z. Skands, *Comput. Phys. Commun.* **191**, 159 (2015), `arXiv:1410.3012 [hep-ph]`.
16. DELPHES 3 Collaboration, J. de Favereau, C. Delaere, P. Demin, A. Giammanco, V. Lemaître, A. Mertens and M. Selvaggi, *JHEP* **02**, 057 (2014), `arXiv:1307.6346 [hep-ex]`.
17. M. Cacciari, G. P. Salam and G. Soyez, *Eur. Phys. J. C* **72**, 1896 (2012), `arXiv:1111.6097 [hep-ph]`.
18. ATLAS Collaboration, G. Aad *et al.*, *Eur. Phys. J. C* **79**, 970 (2019), `arXiv:1907.05120 [hep-ex]`.
19. ATLAS Collaboration, G. Aad *et al.*, *https://doi.org/10.17182/hepdata.91127.v2* (2020).
20. J. Kim, T. G. Lee, J. Kim and H. Jang, *https://doi.org/10.14428/DVN/LYQMUJ* (2020).